A TWO-PARAMETER STUDY OF THE LOCKING REGION OF A SEMICONDUCTOR LASER SUBJECT TO PHASE-CONJUGATE FEEDBACK

KIRK GREEN*, BERND KRAUSKOPF†, AND GIOVANNI SAMAEY‡

Abstract. We present a detailed bifurcation analysis of a single-mode semiconductor laser subject to phase-conjugate feedback, a system described a delay differential equation. Codimension-one bifurcation curves of equilibria and periodic orbits and curves of certain connecting orbits are presented near the laser's locking region in the two-dimensional parameter plane of feedback strength and pump current. We identify several codimension-two bifurcations, including a double-Hopf point, Belyakov points and a T-point bifurcation, and show how they organize the dynamics.

This study is the first example of a two-parameter bifurcation study of a delay system. It was made possible by new numerical continuation tools, implemented in the package DDE-BIFTOOL, and showcases their usefulness for the study of delay systems arising in applications.

Key words. Semiconductor lasers, phase-conjugate feedback, delay differential equations, two-parameter continuation, heteroclinic orbits, T-point bifurcation

AMS subject classifications. 37N20, 34K18, 37G10, 37G20

1. Introduction. The majority of lasers in application today are semiconductor lasers. They can be found, for example, in CD-players, laser printers and in optical communications networks. Semiconductor lasers are so-called Class B lasers, in which the polarization of the electric field can be adiabatically eliminated. As a consequence, they can be described well by three-dimensional rate equations, one for the complex electric field $E(t)$ and one for the population inversion $N(t)$ (the number of excited states that can produce a single photon). It turns out that the phase $\phi(t)$ of the electric field follows the two equations for the optical intensity $P(t) = |E(t)|$ and the inversion $N(t)$. Therefore, a solitary semiconductor laser is essentially a two-dimensional dynamical system that cannot exhibit chaotic dynamics. The only observable dynamical behavior is a damped periodic exchange between the electric field and the inversion. These oscillations are referred to as *relaxation oscillations* in the laser literature (not to be confused with relaxation oscillations in slow-fast systems); see, for example, [26, 38] as an entry point to the theory of semiconductor lasers.

The occurrence of interesting dynamics in a semiconductor laser system requires the addition of one or more degrees of freedom to the rate equations. The good news, from a dynamical systems point of view, is that this is easily achievable with the addition of some form of external influence. This may be due to noise, optical injection from another laser, or delayed optical feedback, the subject of this paper.

Optical feedback results when a part of the solitary laser's output light is fed back into the laser after a delay time τ. This feedback can be unwanted; for example, reflections from a CD or optical fiber can seriously interrupt the proper operation of

*Department of Engineering Mathematics, University of Bristol, Bristol BS8 1TR, UK (kirk.green@bristol.ac.uk).

†Department of Engineering Mathematics, University of Bristol, Bristol BS8 1TR, UK (b.krauskopf@bristol.ac.uk); supported by an EPSRC Advanced Research Fellowship.

‡Department of Computer Science, K. U. Leuven, Celestijnenlaan 200A, 3001 Heverlee, Belgium (giovanni.samaey@cs.kuleuven.ac.be); Research Assistant of the Fund of Scientific Research – Flanders.

the device. However, more recently, it has been demonstrated that chaotic output from a feedback laser can be used in optical encryption schemes [10, 31, 42].

In an experiment, controllable optical feedback is obtained by adding an external mirror to the laser set-up; see already Fig. 2.1. If this mirror is a conventional optical reflector then one speaks of conventional optical feedback (COF), a system that has received much attention due to its relevance for applications, as well as because very complicated dynamics has been found; see, for example, [11, 32]. If the optical feedback comes from a phase-conjugating mirror (PCM) then one speaks of a laser with phase-conjugate feedback (PCF). This is the laser system that we are studying here. It is physically interesting because, unlike in COF, the PCM reverses the phase of the light, so that the reflected wave travels back along the same path as the incident wave. This means that the alignment of the laser beam is not so much of an issue. Furthermore, perturbations to the light front on the way to the PCM are undone on the way back. Also in the PCF laser many interesting dynamical regimes have been identified; see, for example, [1, 12, 16, 24]; more details can be found in Sec. 2.

Mathematically, optical feedback is described by adding a delay term to the equation describing the electric field. This implies that the system is described by a delay differential equation (DDE) with an infinite-dimensional phase space. Consequently, lasers with optical feedback may exhibit very complicated dynamics, and their analysis is quite hard. Until quite recently, the analysis of the linear stability of steady states and direct simulation of the equations were essentially the only tools to study the dynamics of DDEs arising in applications. However, this is changing with the introduction of advanced tools allowing detailed bifurcation studies of DDEs. These consist of (a) the publicly available Matlab Package DDE-BIFTOOL for numerical bifurcation analysis (see [8] and Sec. 4 below), and (b) an algorithm, using DDE-BIFTOOL to obtain the necessary starting data, to compute unstable manifolds of saddle periodic orbits in a suitable Poincaré section [25]. (This algorithm was used in Ref. [19] to identify the break-up of a torus in the PCF laser and its subsequent disappearance in a crisis bifurcation [19].)

The package DDE-BIFTOOL is our main tool here. It allows the continuation of steady states and periodic solutions in (systems of) DDEs, irrespective of their stability, and detects their local bifurcations. Codimension-one bifurcations of steady states can be continued in two parameters, but at present codimension-one bifurcations of periodic orbits can only be detected, not followed; see Sec. 4 for details. DDE-BIFTOOL is still under development with the aim of reaching the same functionality as continuation packages for ordinary differential equations (ODEs), such as the well-known continuation package AUTO [6]. The latest release of DDE-BIFTOOL allows the continuation of connecting orbits [36], much in the same way as the HomCont part of AUTO; see Sec. 4.1.

Continuation techniques have not yet been widely used to study the dynamics and bifurcations in DDEs arising in applications. First examples include the series of papers [21, 34, 35] in which connecting bridges of periodic solutions in the COF laser were studied, and similar work on a vertical-cavity surface-emitting laser [37]. Continuation studies of the PCF laser can be found in Refs. [17, 18, 19].

So far all continuation studies mentioned above follow steady states and periodic orbits as a single parameter is changed (usually the strength of the feedback). This is also the case in Ref. [18] where the locking range of the PCF laser was studied in detail. This revealed regions of bistability associated with a saddle-node bifurcation, a Hopf bifurcation and heteroclinic connections. The next logical step in the study of

DDEs is to construct a full two-dimensional bifurcation diagram.

In this paper we do just this: we present a consistent two-dimensional bifurcation diagram near the locking region of the PCF laser in the plane of feedback strength versus pump current. (These parameters are physically natural and were also used in an experimental overview of the COF laser in Ref. [9].) We follow bifurcations of steady states and connecting orbits in two-parameters. We make a first attempt at mapping bifurcations of periodic orbits by detecting a sufficient number of individual bifurcation points at appropriate values of the parameters. We identify several codimension-two bifurcations, most importantly, a double-Hopf point, a Belyakov point and a bifurcation of heteroclinic orbits known as a T-point. We show how the dynamics of the PCF laser near the locking region are organized around these points.

The paper is organized as follows. In Sec. 2 we introduce the rate equations for the PCF laser. In Sec. 3 we give a brief introduction to the basic theory of DDEs. The capabilities of the continuation package DDE-BIFTOOL, in particular with respect to connecting orbits, are introduced in Sec. 4. In Sec. 5 we present a two-parameter bifurcation analysis of the steady states and a heteroclinic orbit involved in the locking mechanisms of the PCF laser. To allow for a better comparison with previous studies, we also present one-dimensional cross sections through the bifurcation diagram for fixed values of the pump current. In Sec. 6 we look more closely at the bifurcations of steady states and continue the branch of heteroclinic orbits involved in the locking mechanism all the way to its end in a codimension-two bifurcation of heteroclinic orbits known as a T-point. The heteroclinic orbits along this branch are studied in Sec. 7 where we also identify a codimension-two Belyakov point. In Sec. 8 we map out bifurcations of periodic orbits near the locking region. Finally, in Sec. 9 we draw conclusions and discuss future work.

2. Phase-conjugate feedback. Our object of study is a semiconductor laser with phase-conjugate feedback from a phase-conjugate mirror, schematically shown in Fig. 2.1. A PCM can be made by utilizing a number of nonlinear optical processes, including stimulated Brillouin scattering, backward stimulated Raman scattering and three-wave down conversion [12]. Probably the most common way of making a PCM is to use degenerate four-wave mixing in which three input waves mix to produce a fourth output wave. Two of the input waves are counter-propagating pump waves from, for example, additional semiconductor lasers. The third wave is the incident wave, which may enter at any angle to the pump waves. These three waves couple through a third-order susceptibility $\chi^{(3)}$ and produce a fourth wave, phase-conjugated to the incident wave. This phase-conjugated wave may be more intense than the incident wave due to additional gain provided by the pump waves [38].

In contrast to conventional optical feedback, the laser light is wave-front inverted at the PCM. The return conjugated wave retraces the path of the incident wave and, therefore, the system is self-aligning. Any distortions of the incident wave between its source and the PCM are undone on the return trip [12]. This produces a highly focused beam [12] that is of considerable advantage when stable output is desired, such as, in mode locking [15] and phase locking, where PCF has been shown to reduce the laser noise considerably [1, 16, 39].

Mathematically, a single-mode semiconductor laser subject to weak (instantaneous) phase-conjugate feedback can be described by the three-dimensional delay differential system

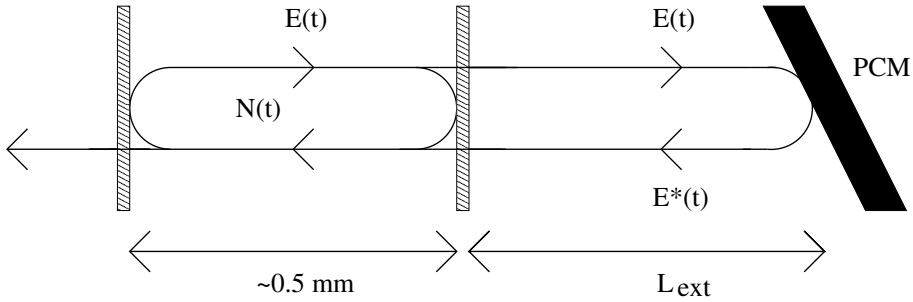

FIG. 2.1. *Sketch of a semiconductor laser with phase-conjugate feedback.*

$$\frac{dE}{dt} = \frac{1}{2}\left[-i\alpha G_N(N(t)-N_{\rm sol}) + \left(G(t)-\frac{1}{\tau_p}\right)\right]E(t) + \kappa E^*(t-\tau)\exp[2i\delta(t-\tau/2)+i\phi_{\rm PCM}]$$
$$\frac{dN}{dt} = \frac{I}{q} - \frac{N(t)}{\tau_e} - G(t)\,|E(t)|^2 \tag{2.1}$$

for the evolution of the slowly varying complex electric field $E(t) = E_x(t) + iE_y(t)$ and the population inversion $N(t)$ [16, 24]. In system (2.1), nonlinear gain is included as $G(t) = G_N(N(t) - N_0)(1 - \epsilon P(t))$, where $\epsilon = 3.57 \times 10^{-8}$ is the nonlinear gain coefficient and $P(t) = |E(t)|^2$ is the intensity. Parameter values are set to realistic values corresponding to a Ga-Al-As semiconductor laser [16, 24], namely, the linewidth enhancement factor $\alpha = 3$, the optical gain $G_N = 1190\,\mathrm{s}^{-1}$, the photon lifetime $\tau_p = 1.4\,\mathrm{ps}$, the magnitude of the electron charge $q = 1.6 \times 10^{-19}\mathrm{C}$, the electron lifetime $\tau_e = 2\mathrm{ns}$, and the transparency electron number $N_0 = 1.64 \times 10^8$. Further, $N_{\rm sol} = N_0 + 1\,/\,(G_N\tau_p)$. The constant phase shift $\phi_{\rm PCM}$ at the PCM and the detuning parameter δ were both set to zero, as is common in the field [16, 24]. Therefore, the feedback term in system (2.1) reduces to $\kappa E^*(t-\tau)$ and involves the complex conjugated electric field E^*, the feedback rate κ and the external cavity round-trip time τ. For one-parameter studies of (2.1), we fix τ at the realistic value $\tau = 2/3\,\mathrm{ns}$, corresponding to an external-cavity length of $L_{\rm ext} \approx 10\,\mathrm{cm}$, and consider the bifurcation parameter $\kappa\tau$; for two-parameter studies we also free the pump current I.

System (2.1) has $\mathbb{Z}_2$-symmetry under the transformation $(E, N) \to (-E, N)$, where the symmetry group is $\mathbb{Z}_2 = \{1, -1\}$. This corresponds to a rotation over π of the complex E-plane, so that any attractor (or other invariant set) is either symmetric, or has a symmetric counterpart. This symmetry allows the possibility of symmetry-breaking and symmetry-restoring bifurcations [24, 27], and also implies restrictions on the types of bifurcations of periodic orbits. For example, symmetric orbits cannot undergo period-doubling bifurcations [28].

It was shown in Ref. [24] that the general picture of the dynamics of the PCF laser is that of stable periodic operation interspersed with 'bubbles' of more complicated, chaotic dynamics. In Ref. [17], these periodic solutions were shown to be connected to a steady state solution. This steady state solution represents a frequency match between the solitary laser and the pump lasers used in the four-wave mixing [38].

Here, the laser is frequency locked and phase locked. In this region the laser phase no longer undergoes diffusion, resulting in an extremely narrow line-width which has been shown to remain stable even with the addition of noise from spontaneous emission [1, 16, 39]. The region in which this stable locked solution exists is called the *locking region* of the PCF laser.

3. Background on DDEs. System (2.1) is a delay differential equation with an infinite-dimensional phase space. As the reader may be unfamiliar with the theory of DDEs, we now give a brief introduction; see [5, 22, 23] for further details.

Models featuring a delay can be found in many areas of science, for example, in biology [33], control theory [14] and, as we have seen, laser physics [26]. They lead to a mathematical description by a DDE which, in its simplest form of a single fixed delay $\tau \in \mathbb{R}$, takes the form:

$$\frac{dx(t)}{dt} = F(x(t), x(t-\tau), \eta) \tag{3.1}$$

where

$$F : \mathbb{R}^n \times \mathbb{R}^n \times \mathbb{R}^p \to \mathbb{R}^n$$

is differentiable and $\eta \in \mathbb{R}^p$ is a multi-parameter. We consider here only the case of one fixed delay. This is not an over-simplification; for example, both the COF laser and the PCF laser introduced in Sec. 2 are of this important class. We remark, however, that the continuation methods described in Sec. 4 also work for a finite number of fixed delays and even for certain state-dependent delays [30].

The *phase space* of (3.1) is the infinite-dimensional space of continuous functions $\mathcal{C}$ over the delay interval $[-\tau, 0]$ with values in $\mathbb{R}^n$. The space $\mathbb{R}^n$ is called the *physical space*; for example, it is (E, N)-space in system (2.1). A *point* $q \in \mathcal{C}$ is a continuous function

$$q : [-\tau, 0] \to \mathbb{R}^n \, .$$

We call $q(0)$ the *head* of q and $\{q(t) \mid t \in [-\tau, 0)\}$ its *history*. The evolution of a point $q \in \mathcal{C}$ after time $t \geq 0$ is given by the *evolution operator*

$$\Phi^t : \mathcal{C} \to \mathcal{C} \, .$$

A *solution* of (3.1) is a function

$$x : [0, \infty) \to \mathbb{R}^n \, , \quad t \mapsto \Phi^t(x_0)$$

for some initial point $x_0 \in \mathcal{C}$.

A *steady state* (or equilibrium) of (3.1) is a point x_0 such that $x_0(t) \equiv \bar{x}_0$ for all $t \in [-\tau, 0]$ and fixed $\bar{x}_0 \in \mathbb{R}^n$. In other words, $F(\bar{x}_0, \bar{x}_0, \eta^*) = 0$ (for some fixed η^*) and $\Phi^t(x_0) = x_0$ for all $t > 0$. The stability of x_0 is given by the linearization (acting on a point $x \in \mathcal{C}$)

$$DF(x_0, \eta^*)\, x = A_1(\bar{x}_0, \eta^*)x(t) + A_2(\bar{x}_0, \eta^*)x(t-\tau) \tag{3.2}$$

around x_0. Here, using $u, v \in \mathbb{R}^n$ as the arguments of $F(u, v, \eta)$,

$$A_1(\bar{x}_0, \eta^*) := \left.\frac{\partial F(u, v, \eta)}{\partial u}\right|_{(\bar{x}_0, \bar{x}_0, \eta^*)} \text{ and } \quad A_2(\bar{x}_0, \eta^*) := \left.\frac{\partial F(u, v, \eta)}{\partial v}\right|_{(\bar{x}_0, \bar{x}_0, \eta^*)} . \tag{3.3}$$

When we define the $n \times n$ matrix Δ as

$$\Delta(x_0, \eta^*, \lambda) := \lambda I - A_1(\bar{x}_0, \eta^*) - A_2(\bar{x}_0, \eta^*) e^{-\lambda\tau} \tag{3.4}$$

then the eigenvalues are given as the roots of the the *characteristic equation*

$$det(\Delta(x_0, \eta^*, \lambda)) = 0. \tag{3.5}$$

It is a crucial property of DDEs with fixed delays that the eigenvalues are discrete and that there are always finitely many eigenvalues with real part larger than γ, for fixed any $\gamma \in \mathbb{R}$. In particular, there are only finitely many unstable eigendirections (associated with eigenvalues with real part greater than zero). As usual, a steady state is called *hyperbolic* if there are no eigenvalues that have zero real part.

A *periodic orbit* is a solution Γ such that $\Phi^{\mathsf{T}}(q) = q$ for some period $\mathsf{T} > 0$ and all $q \in \Gamma$. After choosing a section $\Sigma \in \mathbb{R}^n$ (locally) transverse to Γ, the point $q = \Gamma \cap \mathcal{C}_\Sigma$ is a fixed point of the corresponding Poincaré map P. Here P is defined on the space $\mathcal{C}_\Sigma$ of points in $\mathcal{C}$ with headpoints in Σ, that is,

$$P: \ \mathcal{C}_\Sigma \to \mathcal{C}_\Sigma, \quad q \mapsto \Phi^{t_q}(q)$$

where t_q is the return time to Σ. The stability of Γ is given by its *Floquet multipliers*, which are the eigenvalues of the linearization DP of P at the corresponding fixed point q. The linearization DP can be found by solving the variational equation along Γ. For any fixed radius $r > 0$ there is only a finite number of Floquet multipliers outside a circle of radius r, so that there are always finitely many unstable eigendirections. A periodic point is called *hyperbolic* if there are no Floquet multipliers on the unit circle.

As is the case for ODEs, a local bifurcation occurs when a steady state or a periodic orbit is not hyperbolic. The generic bifurcations are saddle-node and Hopf bifurcations of steady states and saddle-node (or fold), period-doubling and torus (or Neimark-Sacker) bifurcations of periodic orbits.

A solution $x(t)$ of (3.1) at some parameter $\eta = \eta^*$ is called a *connecting orbit* if the limits

$$\lim_{t \to -\infty} x(t) = x^-, \qquad \lim_{t \to +\infty} x(t) = x^+, \tag{3.6}$$

exist, where $x^\pm$ are steady states of (3.1). Connecting orbits are discussed in more detail in Sec. 4.1.

4. Numerical continuation with DDE-BIFTOOL. The continuation package DDE-BIFTOOL [8] has been developed for the numerical bifurcation analysis of DDEs with fixed, discrete delays or state-dependent delays [30]. While a large number of packages exist for the numerical bifurcation analysis of ODEs, for example, AUTO [6] and CONTENT [29], DDE-BIFTOOL is the first publicly available package for the bifurcation analysis of DDEs. Roughly speaking, DDE-BIFTOOL has the same functionality as the early versions of AUTO with new features constantly being added, such as the computation of connecting orbits discussed below in Sec. 4.1.

DDE-BIFTOOL allows the user to find and follow steady states and periodic solutions irrespective of their stability. It also detects the generic codimension one local bifurcations of steady states and periodic orbits by detecting when an eigenvalue of the linearization has a zero real part or is on the unit circle, respectively. The software is able to switch to the continuation of emanating branches of periodic orbits at

bifurcation points (such as a Hopf bifurcation). Furthermore, once a codimension-one bifurcation of a steady state has been detected, it can be followed in two parameters. At present, codimension-one bifurcations of periodic orbits can be detected, but cannot be continued in two parameters. A recent addition to DDE-BIFTOOL is the computation of connecting orbits using projection boundary conditions and their continuation in two parameters [36]. This algorithm is a natural extension of the method that was implemented for the computation of connecting orbits in ODEs in the HomCont [4] extension of AUTO.

The infinite-dimensional nature of DDEs means that the computation of solutions and their stability is far from trivial. To compute the stability of steady states DDE-BIFTOOL approximates an appropriate number of the rightmost roots of the characteristic equation and corrects them by using a Newton's iteration. A steady state is represented by the value of the parameter η, the steady state position $\bar{x}_0$ and the eigenvalues λ_i of this steady state. A saddle-node bifurcation is detected and represented by a null-vector of $\Delta(x_0, \eta^*, 0)$, the matrix defined in (3.4). Similarly, a Hopf bifurcation is represented by the complex null-vector of $\Delta(x_0, \eta^*, i\omega)$ and corresponding frequency ω. To represent and follow periodic solutions orthogonal collocation, based on a piecewise polynomial representation of the solution, is used. A periodic solution is represented by the value of the parameter η, the period T and a time-scaled profile $x^*(t/T)$ on a mesh over the interval $[0, 1]$.

DDE-BIFTOOL can be extended to monitor other quantities that might be of interest to users. One such example was developed and implemented for the analysis in Sec. 7 to find and follow a neutral saddle (-focus) point. This is a steady state solution where the sum of the real parts of the unstable (complex conjugate) eigenvalues $\lambda_{1,2}$ and the leading stable eigenvalue λ_3 is equal to zero. A neutral saddle is represented by the steady state position $\bar{x}_0$, the values of the parameter η, the leading eigenvalues $\lambda_{1,2}$ and λ_3, and their eigenvectors, and is subject to the constraint that $Re(\lambda_{1,2}) + Re(\lambda_3) = 0$. These fields are used as elements inside the branch structure when computing and continuing a neutral saddle point.

4.1. Computing connecting orbits in DDEs. A recent addition to DDE-BIFTOOL is the continuation of connecting orbits [36]. Both homoclinic orbits ($x^- = x^+$ in (3.6)) and heteroclinic orbits ($x^- \neq x^+$ in (3.6)) can be computed and continued as certain system parameters η are varied. This requires finding a good starting solution for a fixed parameter value. For a homoclinic orbit, one can start from a nearby periodic orbit with a sufficiently large period. Heteroclinic orbits can be approximated by using time integration, or by using an extension of the method of successive continuation [7].

A defining condition for a connecting orbit is that it is contained in both the stable manifold of x^+ and in the unstable manifold of x^-. A classical approach in the ODE case is to approximate this condition by truncating the time domain to an interval of length T and to apply (so-called) projection boundary conditions [2]: one end point of the connecting orbit is required to lie in the unstable eigenspace of x^- and the other end point in the stable eigenspace of x^+.

In the implementation this approach was extended to the case of DDEs. Because one needs to provide an initial *function segment* (rather than just an initial value as for ODEs), the boundary conditions need to be written in terms of solution segments. Further, x^+ has infinitely many eigenvalues with negative real parts, so that it is impossible to write the final function segment as a linear combination of all (infinitely many) stable eigenfunctions. Instead, it is required that the end function segment is

in the *orthogonal complement* of all unstable eigenfunctions.

More specifically, the condition for the initial function segment $x_0(\theta)=x(\theta)$, $\theta \in [-\tau, 0]$ can be written as

$$x_0(\theta) = x^- + \epsilon \sum_{k=1}^{s^-} \alpha_k v_k^- e^{\lambda_k^- \theta}, \qquad \left(\sum |\alpha_k|^2 = 1\right)$$

where s^- is the number of unstable eigenvalues λ^-, with corresponding eigenvectors v^-. The α_k are unknown coefficients, and ϵ is a measure for the desired accuracy. An extra condition is added to ensure continuity at $\theta = 0$. As discussed above, we cannot write the end conditions for the final function segment in a similar way. Instead a special bilinear form [22] is used to express the fact that the final function segment is in the complement of the unstable eigenspace of x^+. This leads to s^+ extra conditions:

$$w_k^{+H}(x(T) - x^+) + \int_{-\tau}^{0} w_k^{+H} e^{-\lambda_k^+(\theta+\tau)} A_2(x^+, \eta) \left(x(T+\theta) - x^+\right) d\theta = 0\,.$$

Here s^+ is the number of unstable eigenvalues of x^+, w_k^+ are the left eigenvectors corresponding to the eigenvalues λ_k^+ and the matrix A_2 is defined in (3.3). While this integral condition works well in practice, one slight drawback is that it does not control the distance of the end function segment to the steady state.

Connecting orbits arise in one-parameter families: any time-translate is also a connecting orbit. Therefore, a phase condition needs to be added to pick just one of these orbits. In general, a number s_η of free parameters is required to obtain a generically isolated solution. As a consequence, the equations for x^- and x^+ (steady state equations), and λ_k^- and v_k^- and λ_k^+ and w_k^+ (characteristic equations), have to be added to the defining system. The result is a system of n differential equations, supplemented with $(s^- + s^+)(n+1) + s^+ + 2$ extra equations, resulting in the need for $s_\eta = s^+ - s^- + 1$ free parameters. We end up with a boundary value problem, which we solve by using a collocation method, where the solution is represented as a piecewise polynomial.

5. The locking range. In this section we use the continuation package DDE-BIFTOOL to detect and follow the bifurcations involved in the locking mechanism of the PCF laser. The resulting bifurcation diagram shown in Fig. 5.1 was obtained by starting a two-parameter continuation from bifurcation points identified in one-parameter studies, including the study described in Ref. [18]. Plotted in red are curves of Hopf bifurcations $H_{1,2}$ where each point on the curve represents a steady state with a pair of pure imaginary eigenvalues. The Hopf curves $H_{1,2}$ are drawn dark when they are supercritical (the bifurcating periodic orbit is stable), and are drawn in a lighter tone when they are subcritical (the bifurcating periodic orbit is unstable). In blue are plotted curves of saddle-node bifurcations SN and pitch-fork bifurcations PF_1, in both cases each point represents a steady state with a real eigenvalue equal to zero. Furthermore, we plot a curve of heteroclinic connections Het_1 between two saddle steady states that are each others symmetric counterparts.

The general picture of the locking range of the PCF laser is that it is bounded by the curve of saddle-node bifurcations SN to the left, the (supercritical parts of the) curves of Hopf bifurcations $H_{1,2}$ to the right and a curve of pitchfork bifurcations PF_1 below. Passing through the locking range is a curve of heteroclinic orbits Het_1. The area above the curve Het_1, and between the curves SN and H_2 is a region of

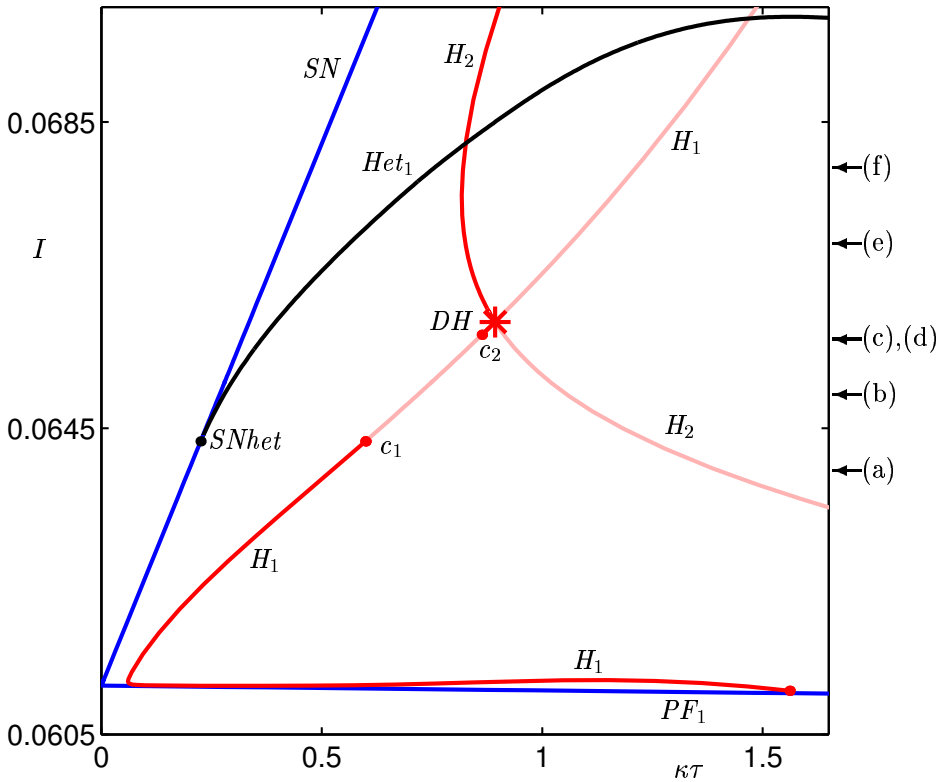

FIG. 5.1. *Bifurcations bounding the locking range of the PCF laser in $(\kappa\tau, I)$-space. The arrows correspond to the one-parameter continuations shown in Fig. 5.2.*

bistability, that is, the periodic orbit involved in the heteroclinic bifurcation Het_1 and the non-symmetric steady states born in the saddle-node bifurcation SN coexist; see already Fig. 5.2 (b) to (f). Note that, when the heteroclinic curve crosses the curve of Hopf bifurcations H_2 there is a second region of bistability, where two stable periodic solutions coexist.

The non-symmetric saddle steady states are born in the saddle-node bifurcation SN together with a pair of non-symmetric stable steady states which correspond to the locked solutions of the PCF laser. These locked solutions are destabilized along the curves of Hopf bifurcations $H_{1,2}$ when they bifurcate with a periodic orbit. Between c_1 and c_2, on H_1, the Hopf bifurcation is subcritical, that is, the bifurcating periodic orbit is unstable. As was shown in Ref. [18], for fixed I, this subcritical Hopf bifurcation leads to a bistability between an attracting steady state and an attracting periodic orbit, and a heteroclinic connection between their respective saddles [18]. This bistability is due to a saddle-node bifurcation of limit cycles SL curve connecting c_1 and c_2, and running parallel to the subcritical part of H_1; see already Fig. 8.1 (b).

The pitchfork curve PF_1 is a bifurcation of the trivial steady state $(E, N) = (0, \frac{I\tau_e}{q})$. Below PF_1, the trivial steady state is stable. It is destabilized at PF_1 when it bifurcates with a pair of non-symmetric stable steady states (the locked solutions). Physically, the PCF laser is in its off-state below PF_1. In this system with $\mathbb{Z}_2$-symmetry the pitchfork bifurcation constitutes the laser threshold, that is, it marks

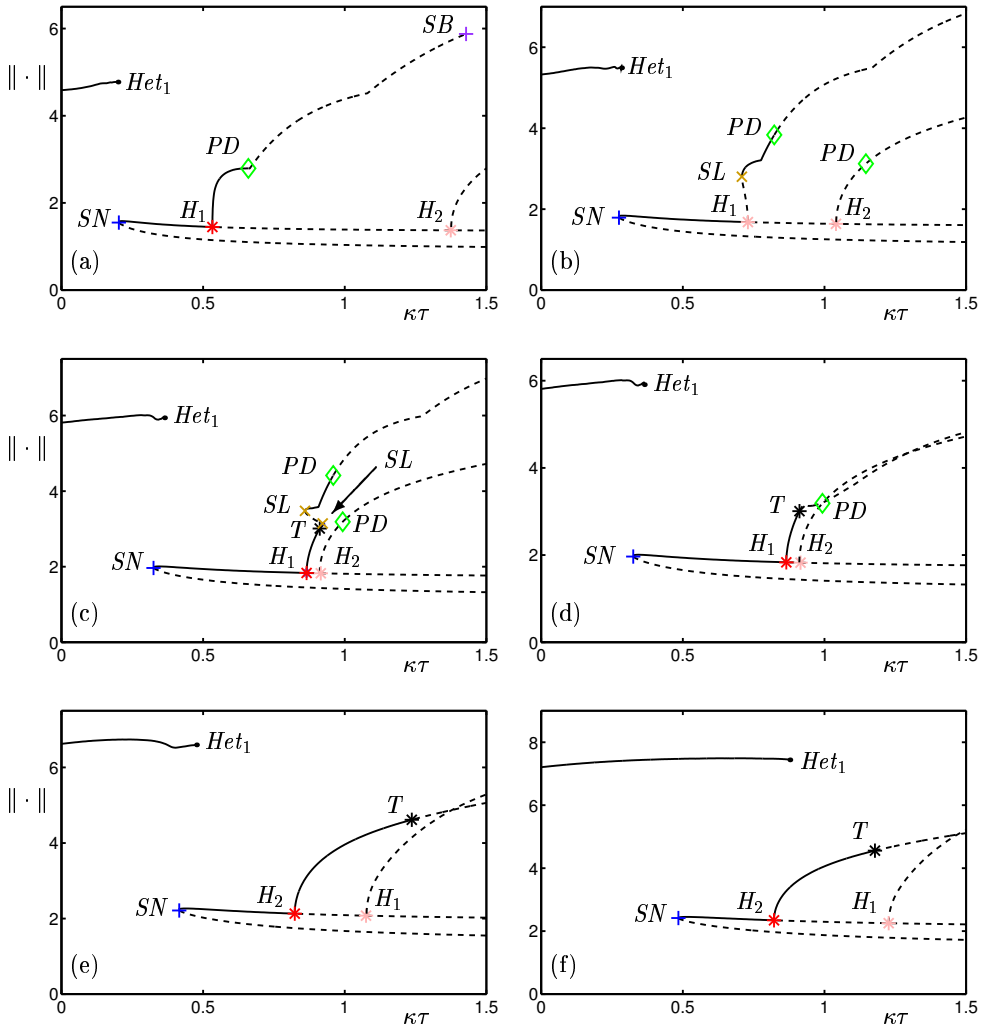

FIG. 5.2. *One parameter continuation of steady states and periodic orbits for fixed pump current I; from (a) to (f) I takes the values* 0.064, 0.065, 0.0657345, 0.0657347, 0.067, *and* 0.068.

the onset of lasing.

The Hopf curves $H_{1,2}$ intersect at the point DH, at $(\kappa\tau, I) \approx (0.893, 0.06589)$, which is a codimension-two double-Hopf bifurcation point where there are two pairs of complex eigenvalues on the imaginary axis [28]. At this bifurcation point the center manifold is four-dimensional, in other words, this bifurcation is only possible in a phase-space of dimension greater than or equal to four. Around a double-Hopf point the system can bifurcate to a number of invariant objects, including two-dimensional tori which may branch to three-dimensional tori [28]. In fact, we will see below that, near the double-Hopf point, a period-doubling route to chaos [18] becomes a route to chaos via the break-up of a torus.

At $(\kappa\tau, I) \approx (0.225, 0.06433)$ the heteroclinic curve Het_1 ends at the saddle-node curve SN at a saddle-node heteroclinic point $SNhet$. Here the saddle-node bifurcation takes place on a codimension-one heteroclinic connection. If we divide out the sym-

metry of system (2.1), this is a saddle-node homoclinic bifurcation [28]. Below the point *SNhet* the saddle-node bifurcation *SN* takes place on a limit cycle [20].

The lower part of the Hopf curve H_1 is seen to bend off and run roughly parallel to the curve PF_1 before terminating. For low values of fixed pump current I, this means that it is possible for the laser to lock and unlock as the value of $\kappa\tau$ is varied; see already Fig. 5.4 (b). However, this effect occurs for a very small range of I and would be extremely difficult to observe experimentally.

We now discuss transitions through the two-dimensional bifurcation diagram in Fig. 5.1 as we vary the value of $\kappa\tau$ for fixed values of I, this is the approach we took in Ref. [18]. The bifurcation diagrams in Fig. 5.2 were obtained with DDE-BIFTOOL and the respective I-values are indicated by the arrows on the right of Fig. 5.1. For steady states we plot $Re(E)$ and for periodic solutions we plot $|\max(Re(E))-\min(Re(E))|$, offset by the $Re(E)$-value of the steady state at the Hopf point. Attracting solutions are drawn as solid curves, while unstable solutions are drawn as dashed curves. By studying the eigenvalues of the system we are able to identify the bifurcations involved. Apart from saddle-node bifurcation *SN*, Hopf bifurcations $H_{1,2}$ and saddle-focus heteroclinic bifurcations Het_1 already shown in Fig. 5.1, we also find saddle-node bifurcations of limit cycles *SL*, period-doubling bifurcations *PD*, symmetry-breaking (or restoring) bifurcations *SB* and torus (or Neimark-Sacker) bifurcations *T*. The different bifurcations are color coded throughout; compare Fig. 5.1, and see already Figs. 5.3, 5.4 (b) and 8.1.

For low values of I [Fig. 5.2 (a)], the saddle-node bifurcation *SN* occurs very close to the saddle-focus heteroclinic bifurcation Het_1. For $I < 0.06433$, the steady state is destabilized in the supercritical Hopf bifurcation H_1. The ensuing periodic solution then undergoes a period-doubling bifurcation *PD*, the first along a route to chaos [18, Fig. 1]. At $I \approx 0.06433$ the Hopf bifurcation H_1 becomes subcritical, for larger values of I [Fig. 5.2 (b)] we observe the emergence of a saddle-node bifurcation of limit cycles *SL*. This is the scenario considered in Ref. [18]. At $I \approx 0.0657345$, the period-doubling route to chaos is preceded by a torus bifurcation *T* and two saddle-node bifurcations of limit cycles *SL*. Consequently, we find a bistability between two stable periodic solutions [Fig. 5.2 (c)]. One of the periodic solutions is born in the Hopf bifurcation H_1 at $\kappa\tau \approx 0.8653$ and is destabilized in the torus bifurcation *T* at $\kappa\tau \approx 0.9118$. The other periodic solution is born in the saddle-node bifurcation of limit cycles *SL* at $\kappa\tau \approx 0.8598$, first identified in Fig. 5.2 (b), and is destabilized in the period-doubling bifurcation *PD* at $\kappa\tau \approx 0.9593$. For $I > 0.0657346$ the route to chaos via the break-up of a torus persists [Fig. 5.2 (d)]. This change, from a period-doubling route to chaos to a route to chaos via the break-up of a torus, appears to be due to the presence of the double-Hopf point. At the double-Hopf point the Hopf curves H_1 and H_2 pass through one another. Fig. 5.2 (e) shows the situation for $I = 0.067$. The first Hopf bifurcation that destabilizes the non-symmetric saddle steady state is now H_2, which leads to a stable periodic orbit that is destabilized in a torus bifurcation *T* at $\kappa\tau \approx 1.236$. As I is increased further there is an increasingly larger region of bistability between a stable periodic solution and the non-symmetric stable steady state at the left boundary of the region of stability. This is a result of the heteroclinic curve Het_1 moving away from the saddle-node bifurcation curve *SN*, and crossing into the locking range. Finally, for $I > 0.068222$ the periodic orbit involved in the heteroclinic bifurcation exists past the first Hopf bifurcation. This is shown in Fig. 5.2 (f) where for $I = 0.068$ we observe a bistability between the periodic orbit involved in the heteroclinic bifurcation and the periodic orbit born in the Hopf bifurcation H_2.

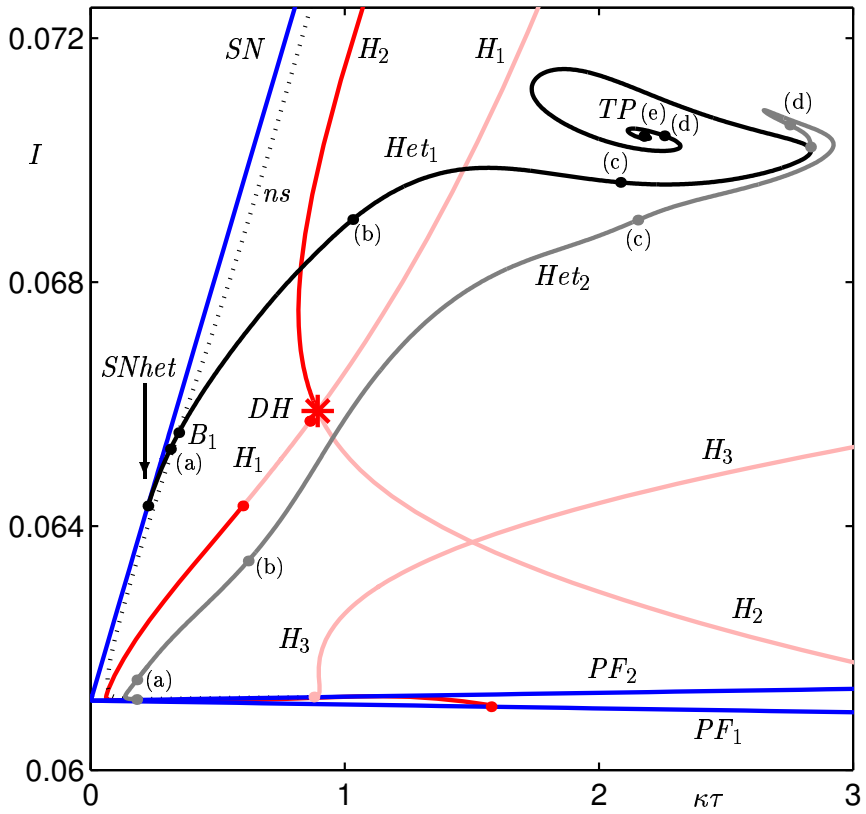

FIG. 5.3. *Bifurcations of steady states in $(\kappa\tau, I)$-space. The labels along the curves $Het_{1,2}$ correspond to phase portraits shown in Figs. 7.1 and 7.3.*

6. Bifurcations of steady states. In Fig. 5.3 we increase the area of $(\kappa\tau, I)$-space under consideration to take a somewhat more global point of view. We follow the curves of saddle-node bifurcations SN, pitchfork bifurcations PF_1, Hopf bifurcations $H_{1,2}$ and heteroclinic bifurcations Het_1 shown in Fig. 5.1 further. We also follow the additional curves of pitchfork bifurcations PF_2, Hopf bifurcations H_3 and heteroclinic bifurcations Het_2, and show a neutral saddle curve ns. This provides a consistent picture of the bifurcations that can be continued, namely, bifurcations of steady states and heteroclinic orbits.

Figure 5.4 shows an enlargement of Fig. 5.3 near the laser threshold, illustrating the interaction of the pitchfork curves $PF_{1,2}$ with the Hopf curves $H_{1,3}$. The steady states in three different regions are sketched, where stable steady states are drawn as blue points and saddle (unstable) steady states are drawn as red points. As was mentioned earlier, below the pitchfork curve PF_1 the trivial steady state is stable [region 1]. Physically, the curve PF_1 marks the onset of lasing of the PCF laser (below this curve the laser is off). At the curve PF_1, the trivial steady state is destabilized and a pair of non-symmetric stable steady states emerge [region 2], these are destabilized at the Hopf curve H_1. The curve of pitchfork bifurcations PF_2 represents another bifurcation of the trivial steady state. At this curve the trivial steady state has a zero eigenvalue, which means that a pair of non-symmetric saddle steady states is born

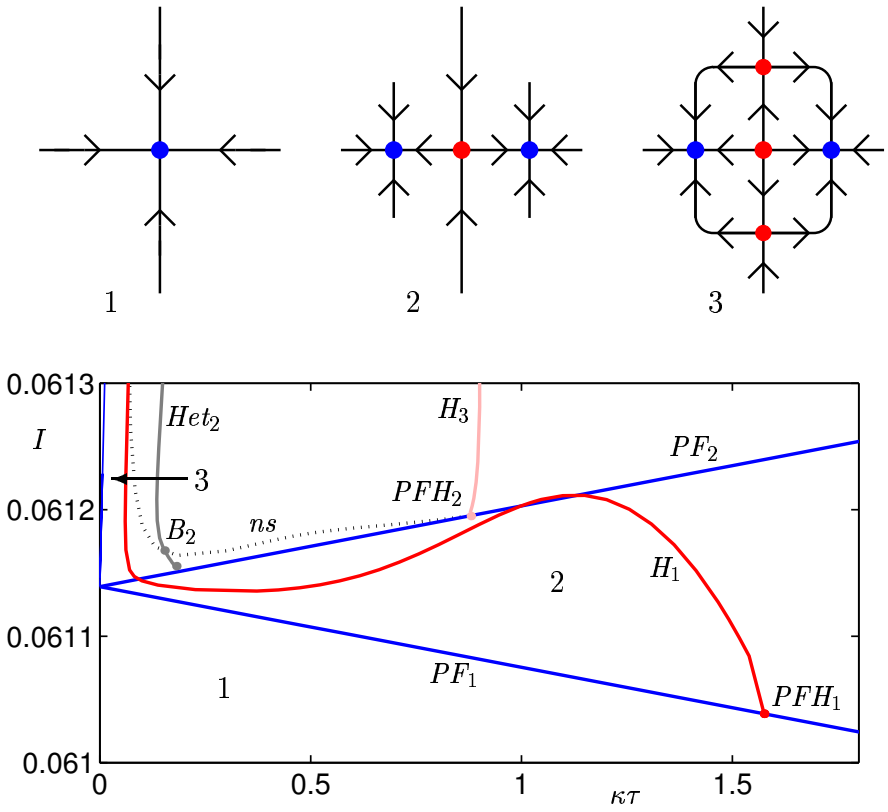

FIG. 5.4. *Enlargement of bifurcation diagram in Fig. 5.3 near the laser threshold, and sketch of stability of steady states in different regions (directions not sketched are attracting).*

[region 3]. These saddles are those involved in the saddle-node bifurcation SN and they appear as the lower branch of saddle steady states identified in Fig. 5.2. At the Hopf curve H_3 this non-symmetric saddle steady state undergoes a Hopf bifurcation, where it bifurcates with a saddle periodic orbit. The codimension-two pitchfork-Hopf bifurcation points $PFH_{1,2}$ represent the ends of the Hopf curves $H_{1,3}$, respectively. At a pitchfork-Hopf point the center manifold is three-dimensional, and one finds a real eigenvalue and two pure imaginary eigenvalues on the imaginary axis [28].

The shape of the Hopf curve H_1 means that the laser can lock and unlock for a fixed value of the pump current I as the feedback strength $\kappa\tau$ is varied. For example, for $I = 0.0612$ a locked solution is born in a saddle-node bifurcation SN at $\kappa\tau \approx 0.00428$. This solution is unlocked (becomes unstable) at the Hopf curve H_1 at $\kappa\tau \approx 0.0606$ and the ensuing solution is once again locked at the Hopf curve H_1 at $\kappa\tau \approx 0.977$. A final intersection with the Hopf curve H_1 at $\kappa\tau \approx 1.227$ results in an unlocked solution. However, we note that this would be extremely difficult to observe experimentally due to the small ranges in the parameters involved.

The curves of heteroclinic bifurcations $Het_{1,2}$ are explained in the next section. We already note that, as is to be expected, they end at the curves SN and PF_2 where the non-symmetric saddle steady states involved in the heteroclinic orbits are born.

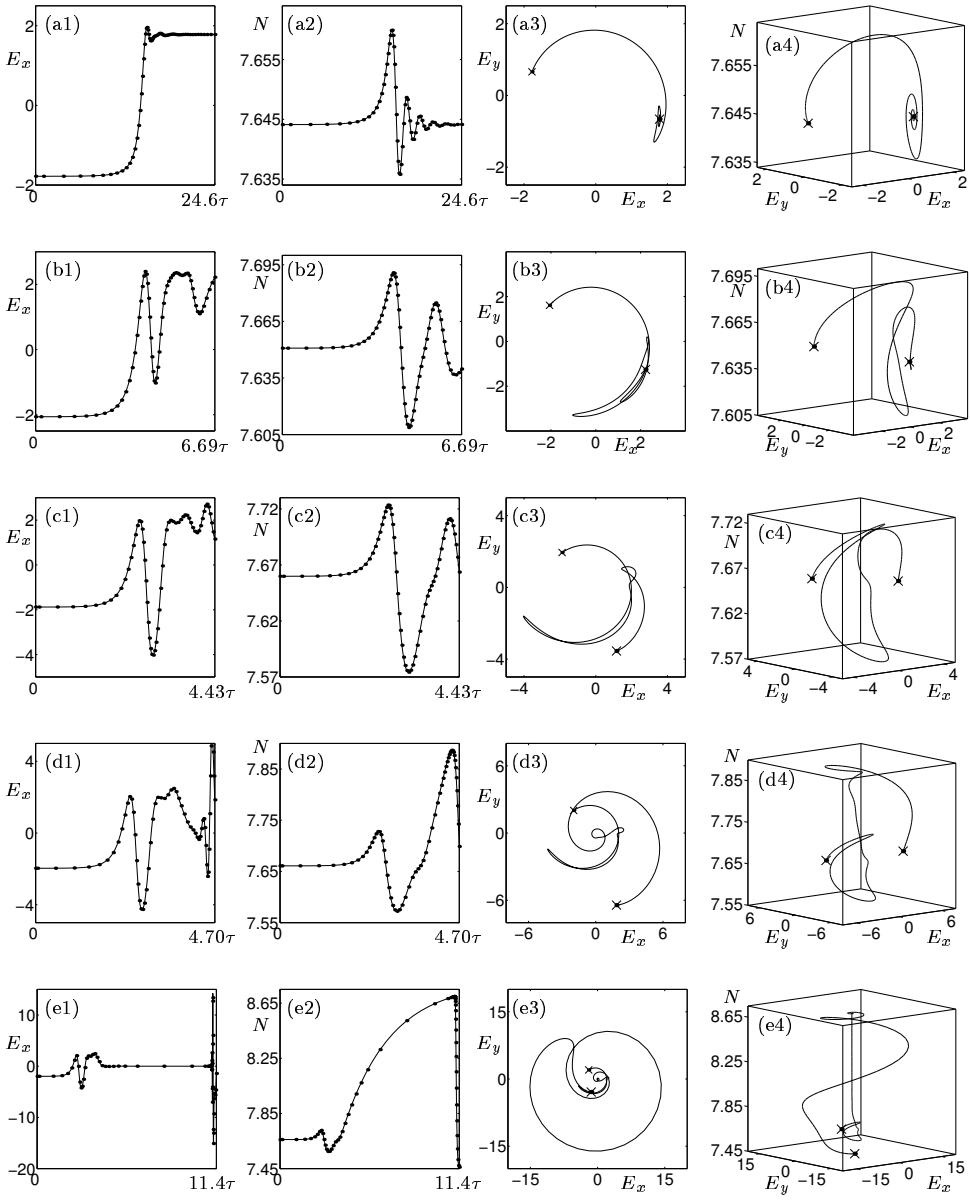

FIG. 7.1. *Heteroclinic orbits along the curve Het_1; from (a) to (e) $(\kappa\tau, I)$ takes the values* $(0.314, 0.065264)$, $(1.303, 0.069026)$, $(2.085, 0.069635)$, $(2.201, 0.070357)$, *and* $(2.177, 0.070394)$. *(The accompanying movie* `Het1.mpeg` *shows the development of the heteroclinic orbits along the branch Het_1 in four panels, top left: position along the curve Het_1 in $(\kappa\tau, I)$-space, top right: the heteroclinic orbit projected onto (E, N)-space, bottom left: E_x on the truncation interval, and bottom right: N on the truncation interval.)*

7. Global bifurcations. Figure 5.3 shows that the curve of heteroclinic bifurcations Het_1 curls up near the point marked *TP*. This indicates that the center point of the spiral is a codimension-two point known as a *T-point* [13]. At *TP* the heteroclinic connection between the two non-symmetric steady states is destroyed. This results in the creation of two heteroclinic orbits from the bifurcating heteroclinic orbit. To show that this is indeed the case we must look at the heteroclinic orbits themselves.

Figure 7.1 shows heteroclinic orbits, calculated with DDE-BIFTOOL, for the parameter values along the curve Het_1 indicated in Fig. 5.3. The first column and second columns show E_x and N, respectively, as a function of time on the truncation interval that was used by the boundary value solver; the third column shows the heteroclinic orbit projected onto the E-plane; and the fourth column shows the heteroclinic orbit projected onto (E, N)-space.

Near the saddle-node bifurcation *SN* [Fig. 7.1 (a)] the orbit is seen to leave one saddle steady state and spiral into its symmetric counterpart; this was also found in Ref. [18]. As one moves along the curve Het_1, the heteroclinic orbits start to increase in size in (E, N)-space [Fig. 7.1 (b4) and (c4)]. As the heteroclinic curve Het_1 approaches the T-point *TP* in $(\kappa\tau, I)$-space, the heteroclinic orbits continue to grow in (E, N)-space [Fig. 7.1 (d)] until just prior to reaching the T-point *TP* the orbit is seen to pass very near the origin of the E-plane. At the same time, the value of the inversion N grows [Figs. 7.1 (e1) and (e2)] with a final rapid oscillation before ending up at the other non-symmetric saddle steady state. The maximum value of inversion N reached is very close to the value of N of the trivial steady state [Fig. 7.1 (e4)]. This is a clear indication that we are very near the forthcoming T-point bifurcation. The evolution of the connecting orbits is also shown in a movie accompanying Fig. 7.1.

One can find the new heteroclinic orbits constituting the heteroclinic orbits at the T-point *TP*, that is, connecting the trivial steady state to the non-symmetric steady states, by providing the boundary value solver of DDE-BIFTOOL with the position and stability information of the trivial steady state. As is to be expected at a T-point there is a codimension-two connection from the non-symmetric steady state to the trivial steady state and a codimension-zero connection from the trivial steady state to the symmetric counterpart of the non-symmetric steady state.

Figure 7.2 (a) shows the heteroclinic orbit between the two non-symmetric steady states. As was detailed in Sec. 4.1, the codimension of a heteroclinic orbit is given by the sum of the dimension of the unstable manifold of the end steady state minus the dimension of the unstable manifold of the initial steady state plus one [36]. The non-symmetric steady states have one-dimensional unstable manifolds. Consequently, the heteroclinic orbit (and its symmetric counterpart) shown Fig. 7.2 (a) is of codimension-one. This orbit is seen to start at one of the non-symmetric steady states and then spend much time at the trivial steady state (red part of the orbit) before a sudden oscillation back to the end non-symmetric steady state (blue part of the orbit). These two parts correspond to the two heteroclinic orbits that we find at the T-point. The first of these is shown in Fig. 7.2 (b). The non-symmetric steady states have one-dimensional unstable manifolds and the trivial steady state has a two-dimensional unstable manifold, therefore, the heteroclinic orbit shown in Fig. 7.2 (b) is of codimension-two. This heteroclinic connection only exists at the point *TP*, and its continuation would require freeing a third parameter, which is beyond the scope of this study. The second heteroclinic orbit found at the T-point *TP* is shown in Fig. 7.2 (c). Because the trivial steady state has a two-dimensional unstable manifold and the non-symmetric steady states have one-dimensional unstable manifolds, this

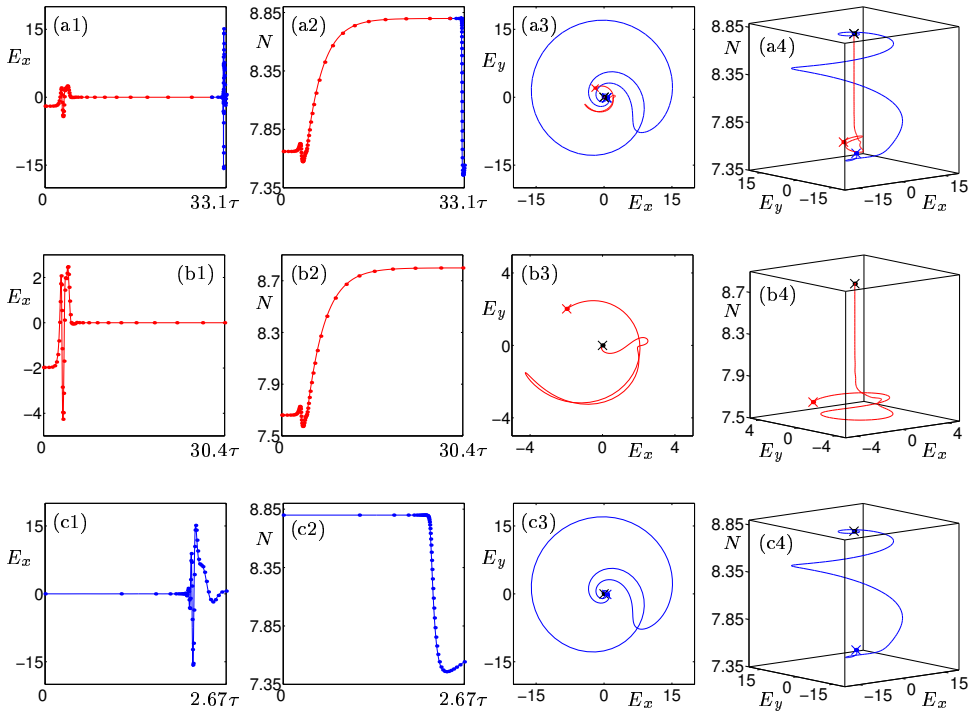

FIG. 7.2. *Codimension-one heteroclinic orbit very close to the T-point TP (a), and the corresponding codimension-two (b) and codimension-zero (c) heteroclinic orbits at the T-point TP.*

heteroclinic orbit is of codimension-zero. In other words, this heteroclinic orbit exists for all values of $(\kappa\tau, I)$ in a local neighborhood of the T-point *TP*.

In Figs. 5.3 and 5.4 (b), the dotted curve *ns* represents a neutral saddle curve, along which the saddle steady states born in the saddle-node bifurcation *SN* have zero saddle quantity, that is, $\sigma = Re(\lambda_{1,2}) + \lambda_3 \equiv 0$, $Re(\lambda_{1,2}) > 0$, $\lambda_3 < 0$. We note that the curve *ns* starts at the pitchfork curve PF_2, the curve in which the non-symmetric saddle steady states associated with the neutral saddle are born; see Fig. 5.4 (b). The curve is seen to intersect the curve of heteroclinic orbits Het_1 at the point B_1, a codimension-two Belyakov point [41]. Along the curve Het_1, the heteroclinic orbits between the saddle-node heteroclinic bifurcation *SNhet* and the Belyakov bifurcation B_1 have a negative saddle quantity corresponding to a bifurcating attracting periodic orbit associated with the heteroclinic bifurcation. Above the Belyakov point B_1 the saddle quantity is positive, this is the case of a chaotic Shil'nikov bifurcation and implies the existence of an infinite number of saddle periodic orbits associated with the heteroclinic bifurcation. Near the Belyakov point B_1 the PCF laser is excitable, that is, if a locked steady state solution is perturbed enough it will produce a large pulse by following the nearby heteroclinic orbit before ending up at the other symmetric locked solution. This may lead to multipulse solutions, as was recently shown for a semiconductor laser with optical injection [41].

The existence of a Belyakov point and a T-point implies that there are infinite sequences of codimension-one homoclinic and heteroclinic orbits in their local vicinities. However, it appears to be very difficult to find and follow these solutions. So far we were unable to find further branches of connecting orbits near the Belykov

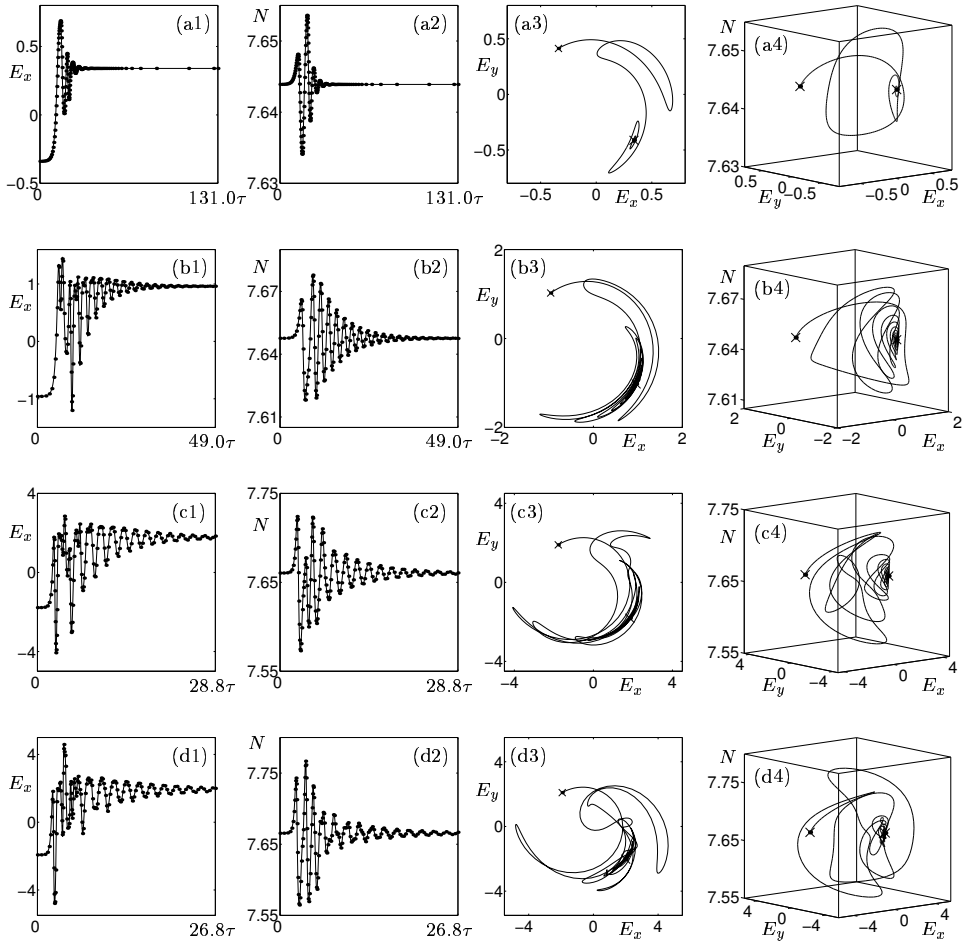

FIG. 7.3. *Heteroclinic orbits along the curve Het_2; from (a) to (d) $(\kappa\tau, I)$ takes the values* $(0.182, 0.061478)$, $(0.620, 0.063430)$, $(2.153, 0.069019)$, *and* $(2.751, 0.070576)$. *(The accompanying movie* `Het2.mpeg` *shows the development of the heteroclinic orbits along the branch Het_2 in four panels, top left: position along the curve Het_2 in $(\kappa\tau, I)$-space, top right: the heteroclinic orbit projected onto (E, N)-space, bottom left: E_x on the truncation interval, and bottom right: N on the truncation interval.)*

point. Near the T-point there are codimension-zero heteroclinic orbits some of which we could find and continue. Theory dictates that the regions where they exist are bounded by curves of codimension-one heteroclinic orbits [13]. Also in this case, we could not locate a starting value which enabled us to follow branches of these orbits.

However, during our investigations, DDE-BIFTOOL detected another branch Het_2 of connecting orbits. This new branch is shown in Fig. 5.3. As is the case for Het_1, it also represents heteroclinic orbits, shown in Fig. 7.3, between the non-symmetric saddle steady states. The curve Het_2 starts at the pitchfork curve PF_2, where the non-symmetric saddle steady states associated with the heteroclinic connection are born; again see Fig. 5.4. The heteroclinic orbit shown in Fig. 7.3 (a) is very close to the pitchfork curve PF_2; note that the non-symmetric steady states, which have just been created, are very close together [Fig. 7.3 (a3)]. As one moves along

Het_2, the orbits oscillate more as they spiral into the end steady state [Fig. 7.3 (b)]. Finally, near the end of the curve Het_2, the damped oscillations become more irregular with the size of the orbit only increasing slightly in (E, N)-space [Fig. 7.3 (c) and (d)]. One sees the emergence of an extra 'arm' of the orbit in Fig. 7.3 (d3). This may be an indication of a bifurcating periodic orbit responsible for the destruction of the curve Het_2 at $(\kappa\tau, I) \approx (2.833, 0.0702)$. It is clear that the heteroclinic curves Het_1 and Het_2 cannot cross, as they involve the same branch of the one-dimensional unstable manifold of the non-symmetric saddle steady states. We note that, unlike it is the case of the curve Het_1, there is no interaction of the curve Het_2 with the trivial saddle steady state. The evolution of the connecting orbits is also shown in a movie accompanying Fig. 7.3.

As is seen in Fig. 5.4, the curve Het_2 crosses the curve ns at the point B_2, another codimension-two Belyakov point. Below the Belyakov point B_2 the heteroclinic orbits along the curve Het_2 have a negative saddle quantity corresponding to a bifurcating attracting periodic orbit, above B_2 the saddle quantity is positive corresponding to an infinite number of bifurcating saddle periodic orbits. Again, we were unable to find further branches of heteroclinic orbits near this Belyakov point.

8. Bifurcations of periodic orbits. In this section we make a first attempt at providing a full two-dimensional picture, including bifurcations of periodic orbits, of the locking range of the PCF laser. We performed a number of one-parameter studies, detected bifurcations of periodic orbits by studying the Floquet multipliers, and plotted the results in $(\kappa\tau, I)$-space.

Figure 8.1 shows colored points indicating bifurcations of periodic orbits. For different values of I a one-parameter continuation of a periodic orbit was performed. By studying the Floquet multipliers of the system the following bifurcations were detected: saddle-node bifurcations of limit cycles SL (yellow points) when a real Floquet multiplier passes through the unit circle at $+1$, period-doubling bifurcations PD (green points) and symmetry-breaking (or restoring) bifurcations SB (purple points), both when a real Floquet multiplier passes through the unit circle at -1, and torus (or Neimark-Sacker) bifurcations T (black points) when a complex pair of Floquet multipliers pass through the unit circle. Figure 8.1 (a) shows bifurcations of the periodic orbit originating from the Hopf curve H_1, while Fig. 8.1 (b) shows bifurcations of the periodic orbit originating from the Hopf curve H_2.

Below the double-Hopf point DH, Fig. 8.1 (a) clearly identifies that a saddle-node bifurcation of limit cycles SL runs close to the curve of subcritical Hopf bifurcations H_1. The stable periodic orbit emerging from the curve SL is destabilized at the curve of period-doubling bifurcations PD (the first in a route to chaos); see Figs. 5.2 (b) and (c). Near the double-Hopf point DH there is an interaction of several bifurcations [28] which we are unable to resolve. (In particular, our calculations suggest that the curve PD does not end at the double-Hopf point DH but turns sharply to the right.) The periodic orbit that is destabilized at PD is destroyed in a symmetry-restoring bifurcation at the curve SB. Above the double-Hopf point DH the bifurcation scenario is very different. The saddle periodic orbits originating from the Hopf curve H_1 are seen to undergo period-doubling bifurcations PD and, in a small range, torus bifurcations T. An obvious question is: why is there a sudden change from a curve of symmetry-breaking bifurcations SB, below the double-Hopf point DH, to a curve of period-doubling bifurcations PD, above the double-Hopf point DH? With the present tools we can not conclusively answer this question. However, initial investigations have revealed a possible heteroclinic connection to a saddle periodic orbit near the

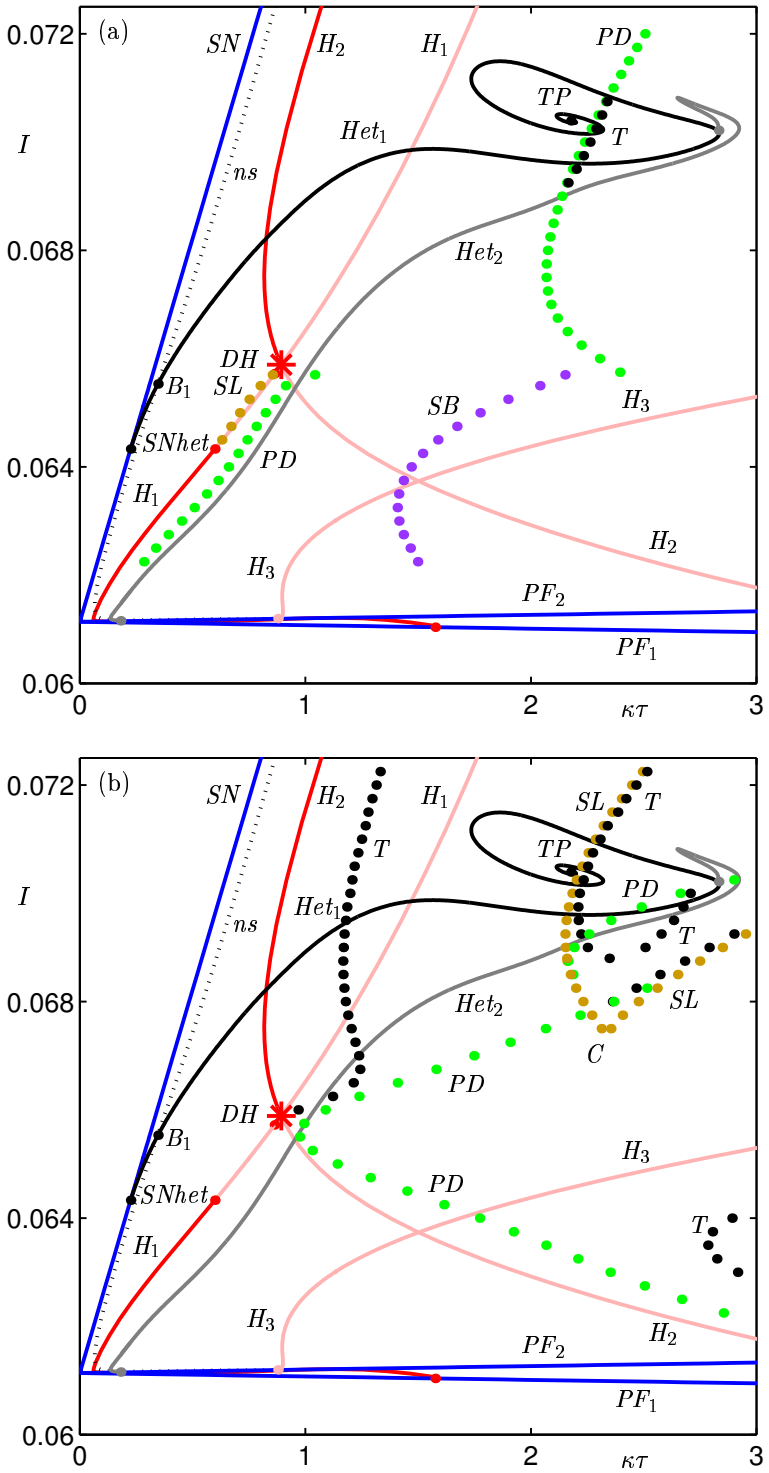

FIG. 8.1. *Bifurcation diagrams in $(\kappa\tau, I)$-space; panel (a) shows bifurcations of periodic orbits originating from the Hopf curve H_1, and panel (b) shows bifurcations of periodic orbits originating from the Hopf curve H_2.*

end points of these curves (around $(\kappa\tau, I) \approx (2.3, 0.0657)$).

The bifurcation scenario of Fig. 8.1 (b) is somewhat clearer. It is now clear that the torus bifurcation T, identified in Figs. 5.2 (e) and (f), originates from the double-Hopf point DH. In the lower half-plane, a large curve of period-doubling bifurcations PD and a smaller curve of torus bifurcations T are identified. The torus bifurcation T originating from the double-Hopf point DH leads to interesting dynamics. Theory states that the curve T comes with narrow resonance tongues, also known as *Arnold tongues* [28]. Inside these tongues we find phase-locked periodic solutions on the torus which lead to additional curves of bifurcations of periodic orbits. Furthermore, away from the curve T the tongues intersect leading complicated bifurcations to chaotic dynamics [28]. A detailed analysis of these resonances is beyond the scope of this chapter.

We also identify a region bounded by curves of saddle-node bifurcations of limit cycles SL. On the curve SL we find a codimension-two cusp point C of saddle-node bifurcations of limit cycles SL at $(\kappa\tau, I) \approx (2.3, 0.0675)$. Such regions are common in periodically driven systems [3] and laser models [40]. Inside this region we identify torus bifurcations T and period-doubling bifurcations PD. It is known that a curve of torus bifurcations can meet a curve of saddle-node bifurcations of limit cycles at a Bogdanov-Takens bifurcation point [28]. Here we also expect a change from supercritical to subcritical of the saddle-node bifurcation of limit cycle curve (this is also known as a 1:1 resonance). Indeed, the lower curve T inside the bounded region is seen to run very close to the curve SL. A period-doubling curve can also meet a torus curve. Again we would expect a change from supercritical to subcritical of the period-doubling bifurcation, a codimension-two point known as a 1:2 resonance [28]. However, at present we can not accurately identify such points and leave a detailed study of bifurcations of periodic orbits as an open problem.

9. Conclusions. We have provided a state-of-the-art two-parameter bifurcation analysis of the locking range of the PCF laser, where we paid particular attention to the computation and continuation of connecting orbits. The general picture is that the locking range is bounded by a saddle-node bifurcation and/or a heteroclinic bifurcation on one side and by Hopf bifurcations on the other; this is consistent with the one-parameter study of Ref. [18]. Pitchfork bifurcations were shown to lead to interactions between the trivial steady state and the non-symmetric steady states of the PCF laser, also forming the laser threshold. A number of codimension-two bifurcations were found to be organizing centers for the dynamics of the PCF laser. These include pitchfork-Hopf bifurcations, a double-Hopf point, a Belyakov point and a T-point bifurcation. Finally, we made a first attempt at mapping out bifurcations of periodic orbits in two parameters. This led to an overall consistent picture, in line with what is to be expected from both theory and studies of other semiconductor laser systems.

Some questions remain about further codimension-two points, in particular a cusp bifurcation and possible Bogdanov-Takens and 1:2 resonance points. Furthermore, it remains a challenge to find connecting orbits in the vicinities of the Belyakov points, and to find the codimnesion-one connecting orbits bounding the regions near the T-point where codimension-zero heteroclinic orbits exist.

To our knowledge what was presented here is the first two-parameter bifurcation study of a DDE with continuation techniques. Our study highlights the usefulness of continuation tools for DDEs and, we hope, may encouragement readers in other fields to use these new techniques.

[1] G. P. Agrawal and G. R. Gray, *Effect of phase-conjugate feedback on the noise characteristics of semiconductor lasers*, Phys. Rev. A, 46 (1992), p. 5890.

[2] W. J. Beyn, *The numerical computation of connecting orbits in dynamical systems*, IMA J. Numer. Anal., 9 (1990), pp. 379–405.

[3] H. W. Broer and B. Krauskopf, *Chaos in periodically driven systems*, in Krauskopf and Lenstra [26], pp. 31–53.

[4] A. R. Champneys, Y. A. Kuznetsov, and B. Sandstede, *A numerical toolbox for homoclinic bifurcation analysis*, Int. J. Bif. Chaos, 6 (1996), pp. 867–887.

[5] O. Diekmann, S. A. Van Gils, S. M. V. Lunel, and H. O. Walther, *Delay Equations: Functional-, Complex-, and Nonlinear Analysis*, vol. 110, Springer-Verlag, 1995.

[6] E. Doedel, T. Fairgrieve, B. Sandstede, A. Champneys, Y. Kuznetsov, and X. Wang, *AUTO 97: Continuation and bifurcation software for ordinary differential equations*, 1997. `http://indy.cs.concordia.ca/auto/main.html`.

[7] E. J. Doedel, M. J. Friedman, and B. I. Kunin, *Successive continuation for locating connecting orbits*, Numer. Algorithms, 17 (1997), pp. 103–124.

[8] K. Engelborghs, T. Luzyanina, and G. Samaey, *DDE-BIFTOOL v2.00: a Matlab package for bifurcation analysis of delay differential equations*, Tech. Rep. TW-330, Department of Computer Science, K. U. Leuven, Belguim, 2000. `http://www.cs.kuleuven.ac.be/~koen/delay/ddebiftool.shtml`.

[9] I. Fischer, T. Heil, and W. Elsässer, *Emission dynamics of semiconductor lasers subject to delayed optical feedback*, in Krauskopf and Lenstra [26], pp. 218–237.

[10] I. Fischer, Y. Liu, and P. Davis, *Synchronization of chaotic semiconductor laser dynamics on subnanosecond time scales and its potential for chaos communication*, Phys. Rev. A, 62 (2000).

[11] A. Gavrielides, *Nonlinear dynamics of semiconductor lasers: Theory and experiments*, in Krauskopf and Lenstra [26], pp. 191–217.

[12] C. R. Giuliano, *Applications of optical phase conjugation*, Physics Today, 34 (1981), pp. 27–35.

[13] P. Glendinning and C. Sparrow, *T-points: A codimension two heteroclinic bifurcation*, Journal of Statist. Phys., 43 (1986), p. 479.

[14] H. Glüsing-Lüerssen, *A behavioural approach to delay-differential systems*, SIAM J. Control Optim., 35 (1997), p. 480.

[15] G. R. Gray, D. H. DeTienne, and G. P. Agrawal, *Mode locking in semiconductor lasers by phase-conjugate optical feedback*, Opt. Lett., 20 (1995), p. 1295.

[16] G. R. Gray, D. Huang, and G. P. Agrawal, *Chaotic dynamics of semiconductor lasers with phase-conjugate feedback*, Phys. Rev. A, 49 (1994), p. 2096.

[17] K. Green and B. Krauskopf, *Bifurcation analysis of frequency locking in a semiconductor laser with phase-conjugate feedback*, Int. J. Bif. Chaos, to appear.

[18] ———, *Global bifurcations and bistability at the locking boundaries of a semiconductor laser with phase-conjugate feedback*, Phys. Rev. E, 66 (2002).

[19] K. Green, B. Krauskopf, and K. Engelborghs, *Bistability and torus break-up in a semiconductor laser with phase-conjugate feedback*, Phys. D, to appear.

[20] J. Guckenheimer and P. Holmes, *Nonlinear Oscillations, Dynamical Systems, and Bifurcations of Vector Fields*, Springer-Verlag, 1993.

[21] B. Haegeman, K. Engelborghs, D. Roose, D. Pieroux, and T. Erneux, *Stability and rupture of bifurcation bridges in semiconductor lasers subject to optical feedback*, Phys. Rev. E, to appear.

[22] J. K. Hale, *Theory of Functional Differential Equations*, vol. 3 of Applied Mathematical Sciences, Springer-Verlag, 1977.

[23] J. K. Hale and S. M. Verduyn Lunel, *Introduction to Functional Differential Equations*, Springer-Verlag, 1993.

[24] B. Krauskopf, G. R. Gray, and D. Lenstra, *Semiconductor laser with phase-conjugate feedback: Dynamics and bifurcations*, Phys. Rev. E, 58 (1998), pp. 7190–7196.

[25] B. Krauskopf and K. Green, *Computing unstable manifolds of periodic orbits in delay differential equations*, J. Comput. Phys., to appear.

[26] B. Krauskopf and D. Lenstra, eds., *Fundamental Issues of Nonlinear Laser Dynamics*, vol. 548, AIP Conf. Proc., 2000.

[27] B. Krauskopf, G. H. M. Van Tartwijk, and G. R. Gray, *Symmetry properties of lasers subject to optical feedback*, Opt. Commun., 177 (2000), p. 347.

[28] Y. Kuznetsov, *Elements of Applied Bifurcation Theory*, Springer, Berlin, 1995.

[29] Y. A. Kuznetsov and V. V. Levitin, *CONTENT: A multiplatform environment for contin-*

uation and bifurcation analysis of dynamical systems, 1997. `ftp://ftp.cwi.nl/pub/CONTENT`.

[30] T. Luzyanina, K. Engelborghs, and D. Roose, *Numerical bifurcation analysis of differential equations with state-dependent delays*, Int. J. Bif. Chaos, 11 (2001), pp. 737–754.

[31] C. R. Mirasso, *Applications of semiconductor lasers to secure communications*, in Krauskopf and Lenstra [26], pp. 112–127.

[32] J. Mørk, B. Tromborg, and J. Mark, *Chaos in semiconductor lasers with optical feedback: Theory and experiment*, IEEE J. Quantum Elec., 28 (1992), p. 93.

[33] J. D. Murray, *Mathematical Biology*, vol. 19, Springer-Verlag, Berlin, 1980.

[34] D. Pieroux, T. Erneux, B. Haegeman, K. Engelborghs, and D. Roose, *Bridges of periodic solutions and tori in semiconductor lasers subject to delay*, Phys. Rev. Lett., 87 (2001).

[35] D. Pieroux, T. Erneux, T. Luzyanina, and K. Engelborghs, *Interacting pairs of periodic solutions lead to tori in lasers subject to delayed feedback*, Phys. Rev. E, 63 (2001).

[36] G. Samaey, K. Engelborghs, and D. Roose, *Numerical computation of connecting orbits in delay differential equations*, Numer. Algorithms, 30 (2002), pp. 335–352.

[37] M. Sciamanna, T. Erneux, F. Rogister, O. Deparis, P. Megret, and M. Blondel, *Bifurcation bridges between external-cavity modes lead to polarization self-modulation in vertical-cavity surface-emitting lasers*, Phys. Rev. A, 65 (2002).

[38] G. H. M. Van Tartwijk and G. P. Agrawal, *Laser instabilities: a modern perspective*, Prog. Quantum Electron., 22 (1998), p. 43.

[39] G. H. M. Van Tartwijk, H. J. C. Van der Linden, and D. Lenstra, *Theory of a diode laser with phase-conjugate feedback*, Opt. Lett., 17 (1995), p. 1590.

[40] S. Wieczorek, B. Krauskopf, and D. Lenstra, *Unnested islands of period-doubling in an injected semiconductor laser*, Phys. Rev. E, 84 (2001).

[41] ———, *Multipulse excitability in a semiconductor laser with optical injection*, Phys. Rev. Lett., 88 (2002).

[42] G. D. V. Wiggeren and R. Roy, *Communication with chaotic lasers*, Science, 279 (1998), p. 1198.